Tom Milligan
Milligan & Associates
8204 West Polk Place
Littleton, CO 80123
(303) 977-7268
(303) 977-8853 (Fax)
TMilligan@ieee.org (e-mail)

A Design Study for the Basic TEM Horn Antenna

R. Todd Lee and Glenn S. Smith

School of Electrical and Computer Engineering, Georgia Institute of Technology
Atlanta, GA 30332-0250 USA
Tel: +1 (404) 894-2922; Fax: +1 (404) 894-4641
E-mail: todd.lee@ieee.org; glenn.smith@ece.gatech.edu

Keywords: Horn antennas; design methodology; antenna radiation patterns; antenna theory

1. Introduction

The transverse electromagnetic (TEM) horn antenna is a popular broadband antenna. The basic antenna is a simple design, consisting only of two triangular metal plates and a feeding structure. Neglecting the feeding structure for the moment, the horn is described completely by only three variables: α, β, and s. As shown in Figure 1, α is the angular width of each plate, β is the angular separation between the two plates, and s is the length, measured from the drive point to a corner of the plate.

Much of the previous research has focused on modifying the antenna's structure to improve the performance. These modifications include resistive loading along the plates [1, 2] and shaping of the plates [3]. What is interesting is that there is very little design information available for the basic TEM horn, as compared to what is available for other horns, such as the sectoral and pyramidal horns [4]. The goal of this paper is to present such information.

2. Characteristic Impedance

In the limit as the antenna becomes infinitely long ($s \to \infty$), a characteristic impedance, Z_c, can be defined for the antenna. This is the impedance of the TEM transmission-line mode on the infinite structure. The characteristic impedance is a function of only the angles α and β [5, 6]. Figure 2 is a graph of the relationship between these angles and the characteristic impedance. In this paper, antennas with the commonly used value $Z_c = 100\,\Omega$ are examined; the angles that determine this impedance lie on the red line in Figure 2.

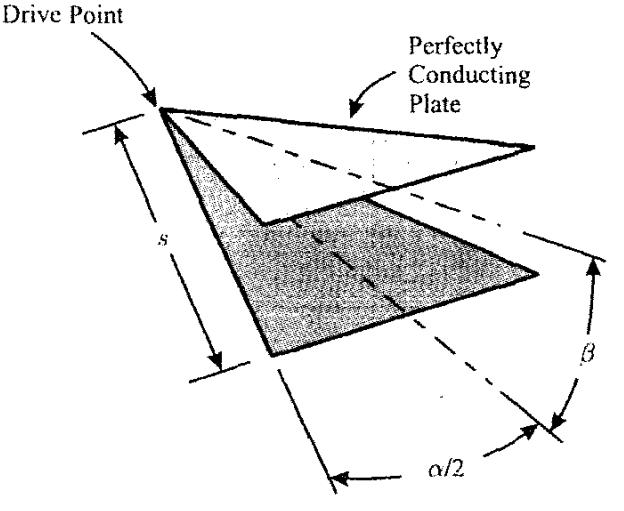

Figure 1. The geometry for the basic TEM horn antenna.

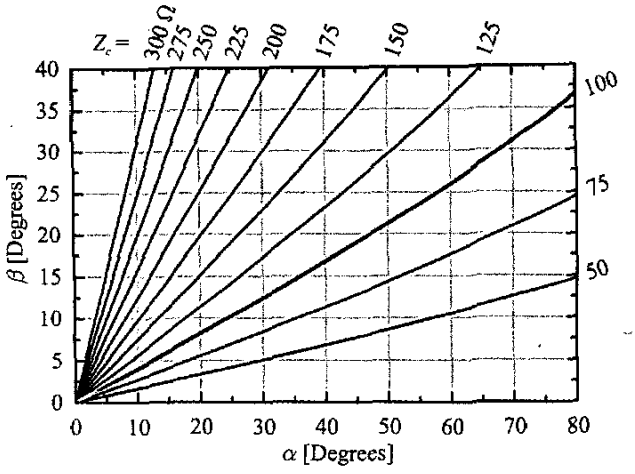

Figure 2. The characteristic impedance, Z_c, of the TEM horn antenna as a function of the angles α and β.

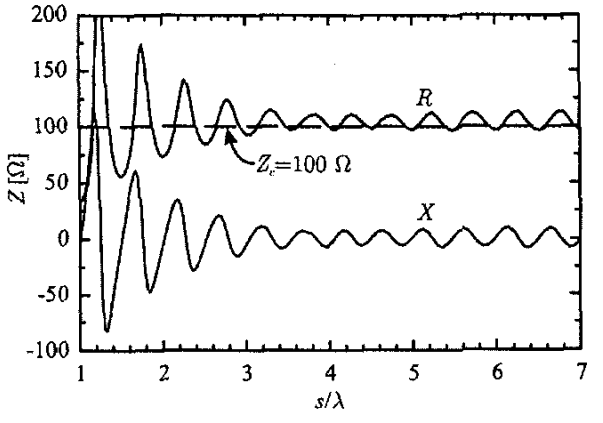

Figure 3. The input impedance, $Z = R + jX$, versus electrical length of the horn antenna. For this antenna, $\alpha = 47.30°$, $\beta = 20°$, and $Z_c = 100\,\Omega$.

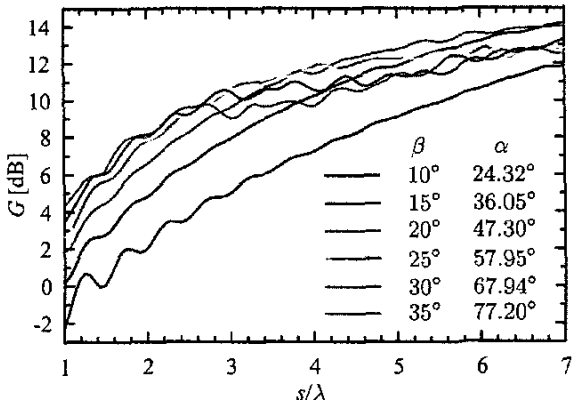

Figure 5. The gain on axis ($\theta = 0°$, $\phi = 0°$) for TEM horn antennas versus electrical length. For all antennas, $Z_c = 100\,\Omega$.

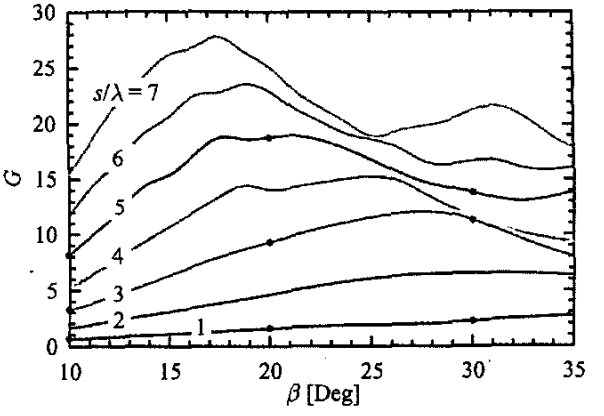

Figure 6. The gain on axis ($\theta = 0°$, $\phi = 0°$) for TEM horn antennas versus the separation angle for the plates. For all antennas $Z_c = 100\,\Omega$. Note that in this graph, a linear scale is used for the gain.

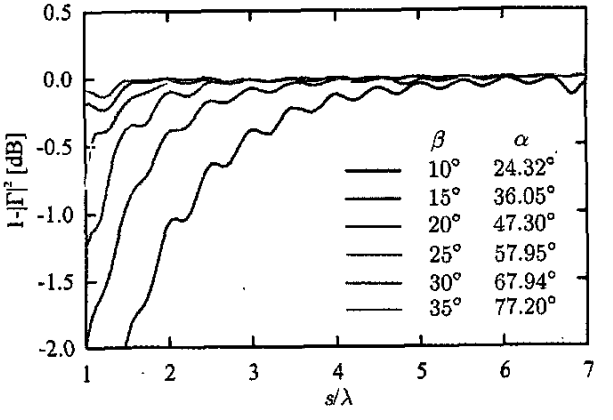

Figure 9. The fraction of the incident power lost due to mismatch, $1-|\Gamma|^2$, for TEM horn antennas versus electrical length. For all antennas, $Z_c = 100\,\Omega$.

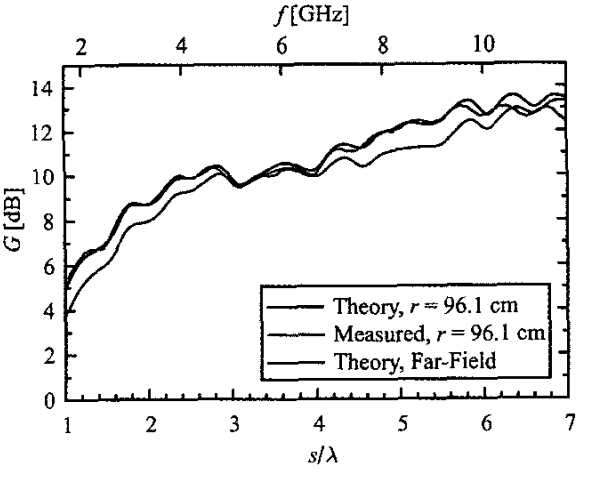

Figure 11. A comparison of theoretical results for the gain with measurements. For this antenna, $\alpha = 71.73°$, $\beta = 32°$, $s = 18$ cm, and $Z_c = 50\,\Omega$ (half antenna).

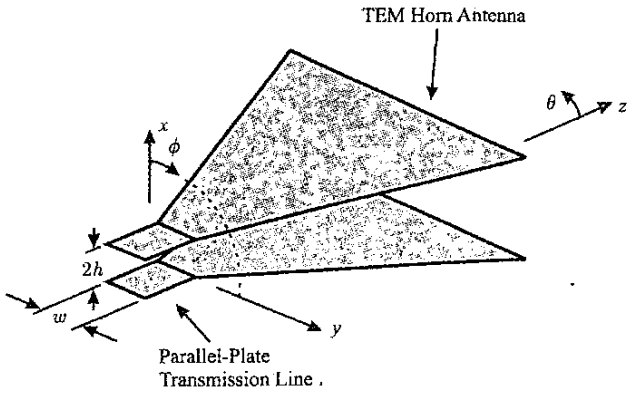

Figure 4a. A TEM horn antenna fed by a parallel-plate transmission line.

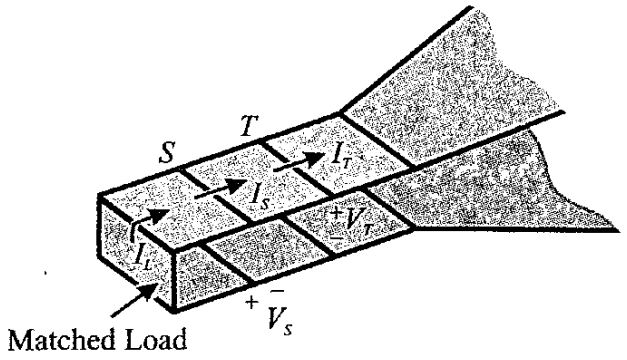

Figure 4b. The detail of the model used for feeding the TEM horn antenna in the numerical simulations.

For an antenna of finite length that is reasonably long, the characteristic impedance of the antenna is a good approximation to the input impedance of the antenna. As an example, the calculated input impedance of an antenna with $\alpha = 47.30°$ and $\beta = 20°$, for which $Z_c = 100\,\Omega$, is shown as a function of the electrical length, s/λ, in Figure 3. The input resistance, R, oscillates around $100\,\Omega$, and the reactance, X, oscillates around $0\,\Omega$. For antennas with $s/\lambda > 3$, the amplitude of the oscillations is fairly small, $\approx \pm 10\,\Omega$. To minimize the reflection at the transmission-line/antenna junction, the characteristic impedances of the feeding transmission line and the antenna are generally chosen to be the same value. With Z_c specified, one of the angles for the horn can be treated as a free variable and the other determined using Figure 2. For this study, the angle β is treated as the free variable, and α is the dependent variable.

3. Model for the Antenna

As mentioned in the introduction, the geometry of the basic TEM horn antenna does not require a particular choice of feeding method. One possibility is to use a parallel-plate transmission line, and then flare the plates outward to form the antenna. This geometry is shown in Figure 4a. In the illustration, the relative size of the transmission line is exaggerated for clarity.

In this study, the antenna is modeled using *FEKO*, a commercial, Method-of-Moments software package [7]. Since this study involves the realized gain of the antenna, an accurate calculation of the input impedance is required. While standard delta-gap models are available for directly calculating the input impedance, these models suffer from the difficulty that the input susceptance depends on the level of the discretization. To avoid this problem, a different feeding scheme is used.

When a two-conductor line is operating below cutoff for all non-TEM modes, the only wave that will propagate down the line is the TEM mode. This means that, regardless of the feed employed, the propagating wave will quickly become a TEM wave. As shown in Figure 4b, delta-gap voltage sources, V_S, are applied at the location marked S on both plates of the transmission line. These sources launch waves in both directions along the transmission line. Away from the sources, the propagating wave is essentially TEM. At the terminals of the antenna, the voltage, V_T, between the plates is computed by integrating the electric field between the plates at the location marked T. Since the Method of Moments program solves for the surface current, the current, I_T, is also available at this location. The input impedance of the antenna, as determined at location T, is then given by

$$Z_{\text{ant}} = \frac{V_T}{I_T}. \tag{1}$$

While a delta-gap source is used in this scheme, this source is used only to inject power into the system; the actual voltage and current are determined away from the source. Therefore, the typical difficulties associated with using delta-gap sources are avoided.

The physical size of the feed and the frequency, f, (wavelength λ) remain constant throughout all of the simulations. The actual length of the antenna is changed to vary quantities such as s/λ. Keeping the physical size of the feed constant insures that any parasitic effects near the feed remain the same for all antennas. Along the transmission-line segment, the width of the plates, w, is $\lambda/10$, and the height, h, is $4.912w$, which sets the characteristic impedance of the parallel-plate transmission line to $100\,\Omega$ [8]. The spacing between the source location and the measurement location is twice the width of the plates. To minimize the unwanted radiation from the section of transmission line, the back end of the line (away from the antenna) is terminated with a matched load: a resistor equal to Z_c.

From the calculated surface current, the radiated electric field, $r\vec{E}$, on axis is found. To convert this field into the gain or realized gain, the total power radiated is required. Ignoring any radiation from the transmission line, this is equal to the power accepted by the antenna at its terminals[1]:

$$P_{\text{rad}} = \frac{1}{2}\text{Re}\left(V_T I_T^*\right). \tag{2}$$

The gain on axis is then given by

$$G = \frac{2\pi\left|r\vec{E}\right|^2}{\eta_0 P_{\text{rad}}}, \tag{3}$$

[1]Another procedure for calculating the radiated power is to subtract the power dissipated in the termination ($P_{\text{diss}} = \frac{1}{2}|I_L|^2 Z_c$) from the power of the gap sources ($P_{\text{in}} = \text{Re}\left(V_S I_S^*\right)$). This method was also tried and gave essentially the same results.

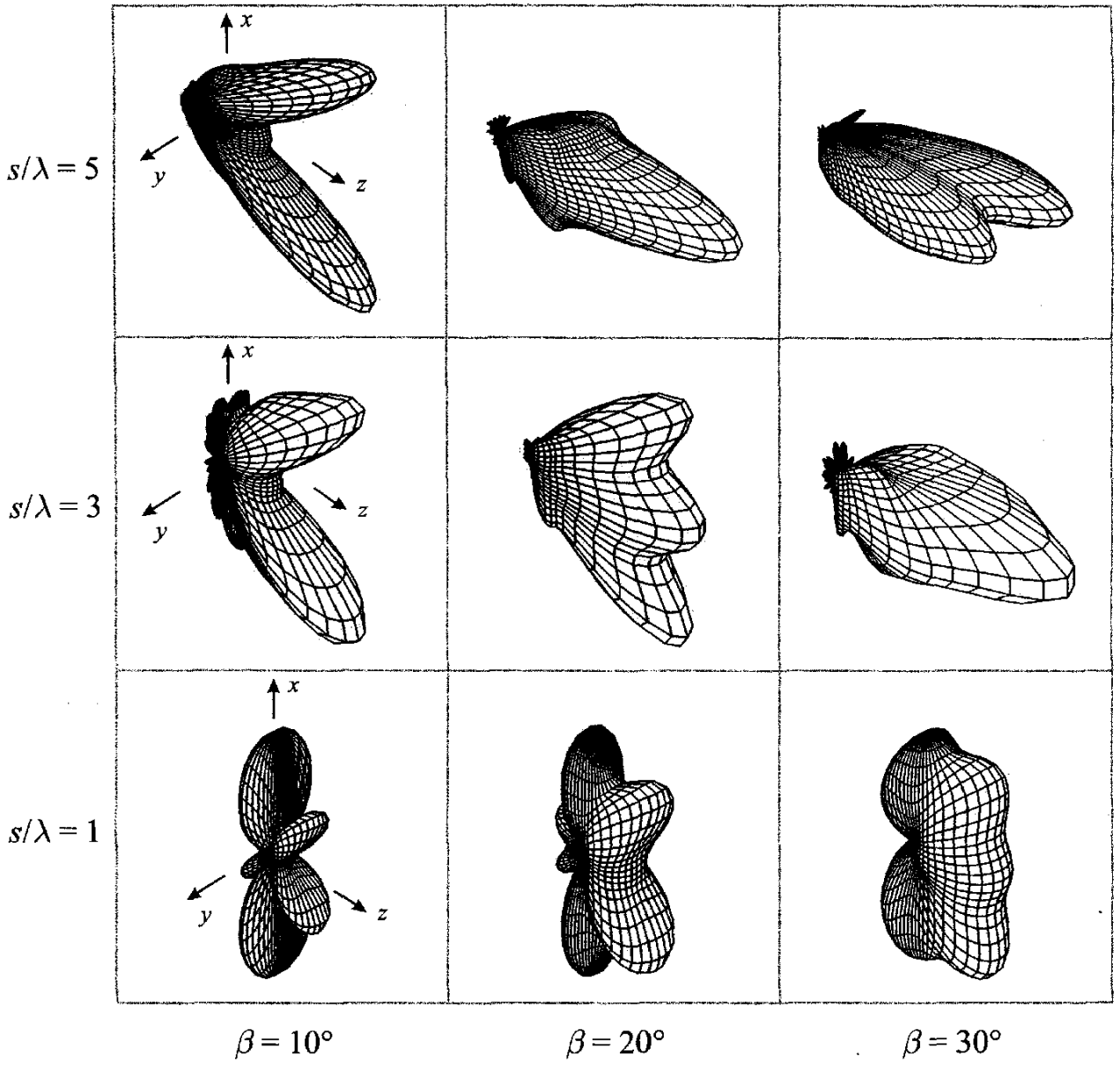

Figure 7. Representative gain patterns for TEM horn antennas. The antenna length increases from $s/\lambda = 1$ to $s/\lambda = 5$ moving from bottom to top, and the separation angle of the plates increases from $\beta = 10°$ to $\beta = 30°$ moving from left to right. For all antennas, $Z_c = 100\,\Omega$.

where η_0 is the wave impedance of free space. Note that the gain, G, is the same as the directivity, D, for the lossless antennas considered here. The realized gain (gain including mismatch) is given by

$$G_r = \left(1 - |\Gamma|^2\right) G, \tag{4}$$

in which Γ is the voltage reflection coefficient in the transmission line.

4. Design Graphs

In this section, the results of a parametric study are presented. The gain and related quantities are determined for different electrical lengths of the antenna, s/λ. The angle β is treated as a parameter over the range $10° \le \beta \le 35°$, and the angle α is determined using the results in Figure 2 so that $Z_c = 100\,\Omega$.

Figure 5 shows the gain on axis ($\theta = 0°$, $\phi = 0°$) versus the electrical length of the antenna, s/λ, for six different values of the separation angle, β. When the small ripples on the curves are ignored, the gain increases with increasing electrical length for any fixed separation angle. For short antennas, $s/\lambda \leq 2$, the gain also increases as the separation angle increases; however, for longer antennas, the gain first increases then decreases with increasing separation angle. To examine this point further, the gain is graphed in Figure 6 as a function of the separation angle, with the electrical length of the antenna as a parameter. For the longer antennas, $s/\lambda \geq 3$, there is a clear peak in the gain, and the peaks occur at progressively smaller separation angles as the electrical length is increased. The causes for this behavior in the gain can be understood by examining radiation patterns for the antenna.

Figure 7 presents an array of three-dimensional gain patterns for the antenna. The orientation for the antenna is as shown in Figure 4a. Each row in Figure 7 shows the gain of an antenna of a particular length ($s/\lambda = 1$, 3, 5) for three different separation angles ($\beta = 10°$, 20°, 30°). The antennas for which patterns are given are indicated by the solid dots in Figure 6.

For the shortest antennas ($s/\lambda = 1$) considered, shown in the bottom row of Figure 7, the radiation pattern is maximum in a direction ($\theta = 90°$, $\phi = 0°$) broadside to the axis of the antenna. Hence, the gain on axis is fairly low for all of the separation angles considered (bottom curve in Figure 6). For the longer antennas ($s/\lambda = 5$), shown in the top row of Figure 7, the radiation pattern is a split beam in the vertical plane at low separation angle ($\beta = 10°$), a directive beam along the axis of the antenna at moderate separation angle ($\beta = 20°$), and finally a split beam in the horizontal plane at high separation angle ($\beta = 30°$). Hence, the gain on axis, Figure 6, exhibits a definite peak when $\beta \approx 20°$. The behavior of the radiation pattern described above is easily explained in terms of traditional antenna analysis.

For determining the pattern in the vertical plane ($\phi = 0°$, 180°), the horn can be likened to a traveling-wave Vee antenna. In the vertical plane, each arm of the Vee produces a pattern with a symmetric pair of lobes, as shown in Figure 8a [9]. Notice that the direction of radiated electric field for each lobe is indicated on the figure. When the separation angle is small, e.g. $\beta = 10°$, the lobes A and A' partially overlap and their fields subtract, as do the fields for lobes B and B'. This produces a pattern in the vertical plane that is a split beam with a null on axis, as shown in Figure 8b for the $\beta = 10°$ case. For larger separation angles, lobes B and A' overlap and their fields add. This produces a pattern in the vertical plane that is a beam with its maximum on axis, as shown in Figure 8b for the $\beta = 20°$ and 30° cases.

For determining the pattern in the horizontal plane ($\phi = 90°$, 270°), the horn can be likened to a uniformly illuminated, rectangular aperture with a quadratic phase variation across its width (y direction). This phase variation is due to the spherical wave in the horn intersecting the aperture plane. As the separation angle increases, the width of the plates also increases, hence the phase variation across the aperture increases. Figure 8c shows patterns in the horizontal plane of a uniform aperture with the same phase variation as the horn. As the separation angle increases from $\beta = 10°$ to $\beta = 30°$, the pattern goes from one with a single lobe to one with a split lobe in the horizontal plane.

Figure 9 shows the fraction of the incident power lost due to mismatch, $1 - |\Gamma|^2$, for these antennas. Notice that the mismatch loss is generally greater the smaller the separation angle. This causes the realized gain, Equation (4), to be significantly lower than the gain, Equation (3), for the shorter antennas, $s/\lambda \leq 2$, with $\beta \leq 20°$. However, once $s/\lambda \geq 3$, all of the antennas are fairly well matched to the transmission line ($|\Gamma| < 0.3$, $1 - |\Gamma|^2 < 0.5\text{dB}$), so the realized gain, Equation (4), and the gain, Equation (3), are essentially the same.

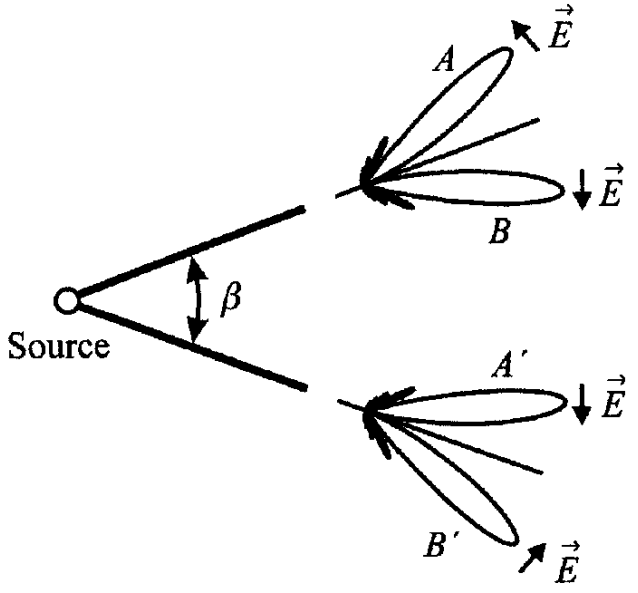

Figure 8a. Explanations for the variation in the gain patterns of the TEM horn antennas with $s/\lambda = 5$: Patterns in the vertical plane ($\phi = 0°$, 180°) for the two traveling-wave elements that make up a Vee dipole antenna.

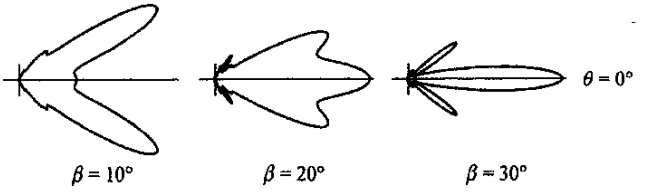

Figure 8b. Explanations for the variation in the gain patterns of the TEM horn antennas with $s/\lambda = 5$: The superposition of the patterns in Figure 8a for various separation angles.

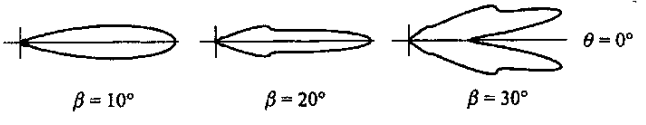

Figure 8c. Explanations for the variation in the gain patterns of the TEM horn antennas with $s/\lambda = 5$: Patterns in the horizontal plane ($\phi = 90°$, 270°) for a uniformly illuminated aperture with a quadratic phase variation across its width that is equal to the phase variation for the TEM horn.

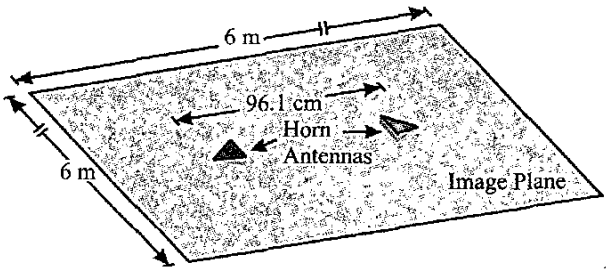

Figure 10a. A schematic drawing showing the measurement system. The drawing is not to scale.

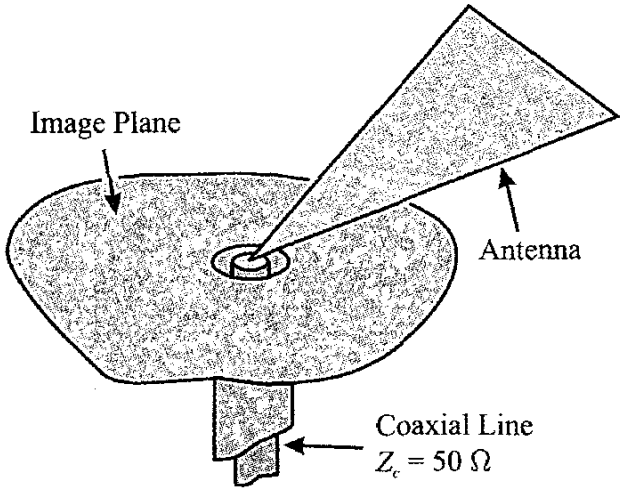

Figure 10b. The detail of the feed region.

5. Comparison with Measurement

Model antennas were constructed, and measurements made on these antennas were used to check the accuracy of the numerical calculations. An image-equivalent was used for the measurements, in which one-half of the antenna was mounted over a large aluminum image plane (6 m × 6 m) and fed through the image plane by a coaxial line with the characteristic impedance $Z_c = 50\,\Omega$. The geometry is shown in Figure 10.

The gain of the antenna was determined using the two-antenna method, with the drive points of the two identical antennas separated by the distance $r = 96.1$ cm [10]. The scattering parameters (S_{11}, S_{21}) for the two-port network formed by the antennas were measured using a vector network analyzer (Agilent 8720D) over the frequency range 50 MHz to 16.05 GHz, and the reflections from the edges of the image plane were removed by windowing in the time domain. The gain of the antenna (excluding mismatch) was then determined from the scattering parameters:

$$G = \frac{4\pi r}{\lambda}\frac{|S_{21}|}{1-|S_{11}|^2}. \qquad (5)$$

The gain calculated from Equation (5) will be independent of the distance between the two antennas, r, only when the antennas are in each other's far zone. This occurs roughly when $r > 2d^2/\lambda$, where d is the maximum dimension of the antennas. For the antennas used, this inequality was not satisfied with $r = 96.1$ cm. As a result, far-zone approximations could not be used when making the numerical computations for comparison with the measurements. Instead, a full model that includes both antennas was required.

In Figure 11, the theoretical (black line) and measured (red line) gains are shown as a function of the electrical size of the antenna, s/λ. These results are for an antenna with $\alpha = 71.73°$, $\beta = 32°$, $s = 18$ cm, and $Z_c = 100\,\Omega$ for the full antenna ($Z_c = 50\,\Omega$ for the half antenna). The theoretical and measured gains are seen to be in good agreement. The small differences (< 1 dB) that do exist at the higher frequencies are probably due to the differences in the feed structures for the theoretical and experimental models: A parallel-plate line is used with the full antenna in the theoretical model, Figure 4a, and a coaxial line is used with the half-antenna in the experimental model, Figure 10b. The theoretical far-zone gain (blue line) is also shown in Figure 11. A comparison of this result with the gain computed at $r = 96.1$ cm (black line) clearly shows the necessity of using the full two-antenna model for the numerical calculations of the gain.

6. Conclusion

In this paper, a design study was performed for the basic TEM horn antenna. In the theoretical model, care was taken to avoid the problems associated with the use of gap sources when calculating the reflection coefficient and input impedance of the antenna. All numerical calculations were made with a program based on the Method of Moments, and the accuracy of the numerical calculations was established with measured results for selected antennas.

In this study, the characteristic impedance for the TEM horn antenna was chosen to be $Z_c = 100\,\Omega$, and the antenna was fed by a parallel-plate transmission line with the same characteristic impedance. The angular separation between the plates, β, was taken to be a variable parameter, and the angle of the plates, α, was always determined so as to keep $Z_c = 100\,\Omega$. Graphs were presented for the gain and the fraction of the incident power lost due to reflection versus the electrical length of the horn, with the angle β as a parameter. Representative field patterns were also presented to show the variation in the directional characteristics of the radiation with the length and angles of the antenna. These graphs should be useful for those wishing to design a basic TEM horn antenna for a particular application.

7. Acknowledgment

The authors would like to thank the Signature Technology Laboratory at the Georgia Tech Research Institute for allowing use of the measurement apparatus. Stephen Blalock of GTRI/STL deserves special thanks for his assistance with the measurement.

This work was supported in part by the John Pippin Chair in Electromagnetics within the School of Electrical and Computer Engineering at the Georgia Institute of Technology.

8. References

1. M. Kanda, "The Effects of Resistive Loading of 'TEM' Horns," *IEEE Transactions on Electromagnetic Compatibility*, **EMC-24**, 2, May 1982, pp. 245-255.

2. K. L. Shlager, G. S. Smith, and J. G. Maloney, "Accurate Analysis of TEM Horn Antennas for Pulse Radiation," *IEEE Transactions on Electromagnetic Compatibility*, **EMC-38**, 3, August 1996, pp. 414-423.

3. R. J. Wohlers, "The GWIA, An Extremely Wide Bandwidth Low-Dispersion Antenna," Calspan Corp., Buffalo, NY, Tech. Rep., 1971.

4. C. A. Balanis, *Antenna Theory: Analysis and Design, Second Edition*, New York, John Wiley & Sons, 1997.

5. F. C. Yang and K. S. H. Lee, "Impedance of a Two-Conical-Plate Transmission Line," *Sensor and Simulation Notes No. 221*, November 1976, US Air Force Research Lab, Kirtland AFB, NM. Available online at http://iget104.et.unimagdeburg.de.

6. R. T. Lee and G. S. Smith, "On the Characteristic Impedance of the TEM Horn Antenna," March 2004, to be published in *IEEE Transactions on Antennas and Propagation.*

7. EM Software & Systems, *FEKO*, August 2003, suite 4.1.

8. M. V. Schneider, "Microstrip Lines for Microwave Integrated Circuits," *Bell System Technical Journal*, **48**, 5, May-June 1969, pp. 1421-1444.

9. G. S. Smith, *An Introduction to Classical Electromagnetic Radiation*, Cambridge, UK, Cambridge University Press, 1997.

10. *IEEE Standard Test Procedures for Antennas*, New York, Institute of Electrical and Electronics Engineers, 1979.

Ideas for Antenna Designer's Notebook

Ideas are needed for future issues of the Antenna Designer's Notebook. Please send your suggestions to Tom Milligan and they will be considered for publication as quickly as possible. Topics can include antenna design tips, equations, nomographs, or shortcuts, as well as ideas to improve or facilitate measurements.

Changes of Address

Information regarding subscription addresses is managed by IEEE headquarters. It is *not* maintained, nor can it be changed, by any member of the *Magazine* staff. If you are a member of the IEEE, your subscription is sent to the address in your IEEE member record. Your record can be updated via the Web at http://www.ieee.org/membership/coa.html. This can also be done by contacting IEEE headquarters: Member Address Records, IEEE Headquarters, 445 Hoes Lane, Piscataway NJ 08855-1331 USA; Tel: +1 (908) 981-0060 or +1 (800) 678-4333; Fax: +1 (908) 981-9667; E-mail: address.change@ieee.org. If you are an institutional or other non-member subscriber, contact IEEE Customer Service at the above address, telephone, and fax numbers; E-mail: customer.service@ieee.org. Do *not* send requests to any member of the *Magazine* staff.